Robust Leader-follower Formation Control of Mobile Robots Based on a Second Order Kinematics Model

LIU Shi-Cai [1, 2] TAN Da-Long [1] LIU Guang-Jun [3]

Abstract In this paper, we study the problem of modeling and controlling leader-follower formation of mobile robots. First, a novel kinematics model for leader-follower robot formation is formulated based on the relative motion states between the robots and the local motion of the follower robot. Using this model, the relative centripetal and Coriolis accelerations between robots are computed directly by measuring the relative and local motion sensors, and utilized to linearize the nonlinear system equations. A formation controller, consisting of a feedback linearization part and a sliding mode compensator, is designed to stabilize the overall system including the internal dynamics. The control gains are determined by solving a robustness inequality and assumed to satisfy a cooperative protocol that guarantees the stability of the zero dynamics of the formation system. The proposed controller generates the commanded acceleration for the follower robot and makes the formation control system robust to the effect of unmeasured acceleration of the leader robot. Furthermore, a robust adaptive controller is developed to deal with parametric uncertainty in the system. Simulation and experimental results have demonstrated the effectiveness of the proposed control method.

Key words Leader-follower robot formation, formation control, robust control, robust adaptive control

1 Introduction

Over the last decade or so, various control techniques have been applied to the formation control design of mobile robots, such as the leader-follower approach[1∼4], virtual leader approach[5, 6], behavior-based approach[7∼10], and bio-inspiration approach[11∼14]. The leader-follower formation control of mobile robots, one of the main approaches in this field, has been studied by many researchers. In a robot formation with leader-follower configuration, one or more robots are selected as leaders, and these are responsible for guiding the formation, and the rest of robots are controlled to follow the leaders and named follower robots. The control objective is to make the follower robots track the leaders with some prescribed offsets.

Desai *et al.*[1∼3] presented a feedback linearization control method for the formation of nonholonomic mobile robots using the leader-follower approach. In [1∼3], the absolute velocity of the leader robot in the local coordinates of the follower robot is treated as a necessary exogenous input for the formation tracking controller. However, the absolute velocities of the leader cannot be measured directly by a local sensor carried by the follower robot. Vidal *et al.*[4, 15] proposed a formation control approach for nonholonomic mobile robots using motion segmentation and visual servoing techniques. In [4, 15], the problem of distributed formation control in the configuration space was translated into separate visual servoing tasks in the image plane of a central-panoramic camera. The motion of the leader robot needed by the tracking controller was estimated by the follower robot through comparing the optical flows of two pixels, are corresponding to a point on the leader and the other to a static point in the environment.

Chiem and Cervera[16] presented a vision-based robot formation approach using the properties of Bézier curves. The global linear velocity of the leader robot was assumed to be constant and known to the follower robot, and only the angular velocity of the follower robot needs to be computed using the curvature of Bézier curves between the two robots. In [17], a dual-mode model predictive controller was proposed for the leader-follower robot formation. The formation controller was designed based on the kinematics model and the feedback linearization controller given in [1∼3]. In [18], a sliding mode controller was designed for the leader-follower robot formation based on the kinematics model given in [2]. The formation control law in this paper requires the absolute velocity and the absolute acceleration of the leader robot, and as it is well konwn, in practive, it is difficult to measure or estimate in practice the absolute acceleration of the leader robot.

Very recently, in [19], a leader-follower formation controller was proposed utilizing only the relative positions between robots, in which the derivatives of the relative positions were estimated using a high-gain observer. A high-gain discontinuous auxiliary control term was added to the control law to stabilize the resulting second order error dynamics in a globally uniformly ultimately bounded manner. The control gains of the discontinuous term were determined by the magnitude of the absolute acceleration of the leader robot and its derivative.

In leader-follower formation control, the most widely used control technique is feedback linearization based on the kinematics model of the system. In this study, we focus on the problem of leader-follower robot formation control with relative motion sensors and develop a control method that does not require a global positioning system or absolute motion sensors.

The first part of this paper presents a second order kinematics model for leader-follower robot formation, which is derived in terms of the relative motion states between the robots and the local motion of the follower robot. The formulation of the proposed model is inspired by the first order kinematics model presented in [1∼3], where the model is described in terms of absolute motion states of the robots. Based on the proposed kinematics model, feedback linearization is implemented to achieve the objective of formation control with relative motion states. However, there is a difficulty in the implementation of feedback linearization. The difficulty is related to the existence of unstable zero dynamics[20]. In practice, the feedback linearization cannot be used if the zero dynamics is unstable. In this study, a stability condition for the zero dynamics of leader-follower robot formation system is derived through constraining the motion of the leader robot and the formation configuration. The stability condition can also be treated as the coopera-

Received August 10, 2006; in revised form January 17, 2007
Supported by National High Technology Research and Development Program of China (863 Program)(2001AA422140)
1. Robotics Laboratory, Shenyang Institute of Automation, Chinese Academy of Sciences, Shenyang 110016, P. R. China 2. Graduate University of Chinese Academy of Sciences, Beijing 100049, P. R. China 3. Department of Aerospace Engineering, Ryerson University, Toronto M5B 2K3, Canada
DOI: 10.1360/aas-007-0947

tive protocol of formation control between robots.

As discussed later in the paper, the internal dynamics of leader-follower robot formation system is only locally stable. When the internal state is in an unstable region, the formation system suffers an increasing perturbation from internal dynamics. To suppress such a perturbation, a robustness inequality is introduced to design the feedback gain. Under the proposed control scheme, the formation tracking error approaches zero even when the internal state is in an unstable region. On the other hand, the convergence of tracking error also forces the internal state to enter the stable region of the internal dynamics. Furthermore, a sliding mode controller is integrated to the feedback linearization controller to compensate for the uncertainty associated with the unknown absolute acceleration of leader robot. The Lyapunov method is used to stabilize the overall system.

In the proposed approach, the commanded acceleration for the follower robot is determined by the control law. However, it is normally not practical for a mobile robot to track an acceleration signal. Instead, in implementation, the acceleration inputs that are determined by the control law are translated into velocity variations by multiplying them with the control period. Hence, the reference velocities for the follower robot, as commonly used in current control methods, can be obtained by adding the velocity variation to the current velocity.

As a further improvement of the proposed robust formation controller, a robust adaptive control scheme is also developed based on the work in [21, 22]. The controller consists of an adaptive control part that serves to deal with parametric uncertainty and a robust control part to compensate for the uncertainty associated with the absolute acceleration of the leader robot.

This paper is organized as follows. In Section 2, the proposed formation kinematics model is derived. The proposed control schemes and robust adaptive control scheme for leader-follower robot formation system are presented in Sections 3 and 4, respectively. Simulations and experimental results are used to illustrate the effectiveness of the proposed control methods in Section 5 and 6, respectively. Finally, conclusions are drawn in Section 7.

2 Formation model formulation

In this section, we formulate the kinematics model of the leader and follower robots in formation. The goal of the formation control is to make the follower robot track the leader robot with desired relative distance and bearing between the robots. As indicated in Fig. 1, the follower robot R_2 follows the leader robot R_1 with a relative distance l_{12} and a relative bearing φ_{12} between the two robots, and a relative motion sensor is mounted at point C on the follower robot R_2.

The kinematics equations of the robots are given by the following equations

$$\begin{pmatrix} \dot{x}_{ci} \\ \dot{y}_{ci} \end{pmatrix} = \begin{pmatrix} \cos\theta_i & -d\sin\theta_i \\ \sin\theta_i & d\cos\theta_i \end{pmatrix} \begin{pmatrix} v_i \\ \omega_i \end{pmatrix} \tag{1}$$

$$\dot{\theta}_i = \omega_i$$

where $(x_{ci} \quad y_{ci})$ are the coordinates of the center of mass P_c in the world coordinates system, and θ_i is the heading angle of the robot. As shown in the Fig. 1, $\overrightarrow{v_i}$ and $\overrightarrow{\omega}_i$ are the linear and angular velocities of the robot R_i, and their scalar representation are given by v_i and ω_i, for $i = 1, \quad 2$, respectively. P_o is the intersection of the axis of symmetry with the driving wheel axis; d is the distance from the center of mass to point P_o; h is the distance from the reference point C to point P_o. The velocity of point C in the local coordinates of robot R_2 is given by $V_2 = [v_2 \quad h\omega_2]^{\mathrm{T}}$. Set $\theta_{12} = \theta_1 - \theta_2$. Then, θ_{12} is the relative orientation between R_1 and R_2, and $\theta_{v_2} = \pi - \varphi_{12} - \theta_{12}$ is the relative bearing between velocity v_2 and line l_{12}.

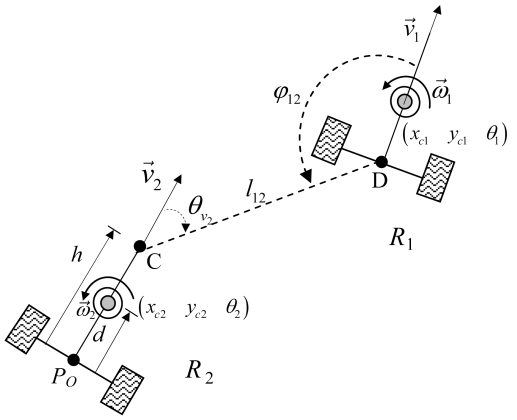

Fig. 1 Two robots using leader-follower controller

2.1 Model formulation of the leader-follower robots system

Similar to [1∼3], the kinematics of the leader and follower robots in formation can be described by

$$M(l_{12}, \theta_{v_2}) \begin{pmatrix} \dot{l}_{12} \\ \dot{\varphi}_{12} \end{pmatrix} - N(l_{12}, \theta_{12}, \theta_{v_2}) \begin{pmatrix} v_1 \\ \omega_1 \end{pmatrix} = \begin{pmatrix} v_2 \\ \omega_2 \end{pmatrix} \tag{2}$$

where the matrices M and N are defined as

$$M = \begin{pmatrix} -\cos\theta_{v_2} & -l_{12}\sin\theta_{v_2} \\ (\sin\theta_{v_2})/h & -(l_{12}\cos\theta_{v_2})/h \end{pmatrix}$$

$$N = \begin{pmatrix} -\cos\theta_{12} & l_{12}\sin\theta_{v_2} \\ -(\sin\theta_{12})/h & (l_{12}\cos\theta_{v_2})/h \end{pmatrix}$$

In (2), the formation motion states have been projected to the local frame of the follower robot R_2. By solving (2), the absolute velocity of the leader robot can be presented by the formation motion states and the absolute velocity of the follower robot

$$N^{-1}\left[M \begin{pmatrix} \dot{l}_{12} \\ \dot{\varphi}_{12} \end{pmatrix} - \begin{pmatrix} v_2 \\ \omega_2 \end{pmatrix}\right] = \begin{pmatrix} v_1 \\ \omega_1 \end{pmatrix} \tag{3}$$

Differentiating (2) and incorporating (3) yields

$$\begin{pmatrix} \dot{v}_2 \\ \dot{\omega}_2 \end{pmatrix} = M \begin{pmatrix} \ddot{l}_{12} \\ \ddot{\varphi}_{12} \end{pmatrix} + C \begin{pmatrix} \dot{l}_{12} \\ \dot{\varphi}_{12} \end{pmatrix} - \dot{\theta}_{12} \begin{pmatrix} h\omega_2 \\ -v_2/h \end{pmatrix} + M \begin{pmatrix} -l_{12}\dot{\varphi}_{12} \\ \dot{l}_{12}/l_{12} \end{pmatrix} \omega_2 + \begin{pmatrix} \delta_1 \\ \delta_2 \end{pmatrix} \tag{4}$$

where the matrix C and the vector $\boldsymbol{\delta}$ are defined as

$$C = \begin{pmatrix} \dot{\theta}_{v_2}\sin\theta_{v_2} & -\dot{\theta}_{v_2} l_{12}\cos\theta_{v_2} - \dot{l}_{12}\sin\theta_{v_2} \\ (\dot{\theta}_{v_2}\cos\theta_{v_2})/h & (\dot{\theta}_{v_2} l_{12}\sin\theta_{v_2} - \dot{l}_{12}\cos\theta_{v_2})/h \end{pmatrix}$$

$$\boldsymbol{\delta} = \begin{pmatrix} \delta_1 \\ \delta_2 \end{pmatrix} = M \begin{pmatrix} -\dot{v}_1 \cos\varphi_{12} \\ (\dot{v}_1 \sin\varphi_{12})/l_{12} - \omega_1 \end{pmatrix}$$

where $\dot{\theta}_{12} = \omega_1 - \omega_2$ and $\dot{\theta}_{v_2} = -\dot{\varphi}_{12} - \dot{\theta}_{12}$ have been used in (4).

Denoting the state variables by $\boldsymbol{q} = (l_{12} \quad \varphi_{12})^{\mathrm{T}}$ and $\dot{\boldsymbol{q}} = (\dot{l}_{12} \quad \dot{\varphi}_{12})^{\mathrm{T}}$, and the input of the robot formation system by $\boldsymbol{u} = (\dot{v}_2 \quad \dot{\omega}_2)^{\mathrm{T}}$, we can rewrite model (4) in the following form

$$\begin{aligned} \boldsymbol{u} &= M(\boldsymbol{q}, \theta_{12})\ddot{\boldsymbol{q}} + C(\boldsymbol{q}, \dot{\boldsymbol{q}}, \theta_{12}, \dot{\theta}_{12})\dot{\boldsymbol{q}} + \\ & \quad G(\boldsymbol{q}, \dot{\boldsymbol{q}}, \theta_{12}, \dot{\theta}_{12}, v_2, \omega_2) + \boldsymbol{\delta}(\dot{v}_1, \dot{\omega}_1, \boldsymbol{q}, \dot{\boldsymbol{q}}) \end{aligned} \quad (5)$$

where the function $G(\boldsymbol{q}, \dot{\boldsymbol{q}}, \theta_{12}, \dot{\theta}_{12}, v_2, \omega_2)$ is defined as

$$G = -\dot{\theta}_{12} \begin{pmatrix} h\omega_2 \\ -v_2/h \end{pmatrix} + M \begin{pmatrix} -l_{12}\dot{\varphi}_{12} \\ \dot{l}_{12}/l_{12} \end{pmatrix} \omega_2 \quad (6)$$

(5) represents the input–output relation for the leader-follower robot formation system, where the outputs are the relative distance and the relative bearing and the relative velocities between robots. The inputs of the system are the absolute accelerations of the follower robot in local coordinates. The relative motion states $\boldsymbol{q}$ and $\dot{\boldsymbol{q}}$ and $\dot{\theta}_{12}$ in (5) can be measured by the relative motion sensors fixed on the follower robot.

The second order kinematics model (5) forms a nonlinear and multivariable system, which allows us to do more rigorous analysis of the performance of control system, and to design robust nonlinear control laws that guarantees the global stability and tracking of more complex trajectories than those for the one order kinematics model.

Remark 1. Using model (5), the relative centripetal and Coriolis accelerations given by $C\dot{\boldsymbol{q}} + G$ in (5) can be computed directly in the light of outputs of the relative motion sensors and the local motion sensor fixed on the follower robot. Furthermore, these relative accelerations can be utilized to linearize the nonlinear leader-follower formation system, as discussed later.

Remark 2. The last term $\boldsymbol{\delta}$ in model (5) represents the effect of the absolute acceleration of leader robot, which is difficult to accurately measure or estimate due to the limitation of the motion sensors and treated as model uncertainty of the system.

2.2 Formulation of internal dynamics

Using (3), the internal dynamics[20] of the leader-follower robot formation system is given by

$$\begin{aligned} \dot{\theta}_{12} &= \omega_1 - \omega_2 \\ &= -\frac{v_1}{h}[\sin\theta_{12} - (\dot{l}_{12}\sin\theta_{v_2} - \dot{\varphi}_{12} l_{12}\cos\theta_{v_2})] + \\ & \quad \omega_1(1 + \frac{l_{12}}{h}\cos\theta_{v_2}) \\ &= -A_\theta \sin(\theta_{12} - \alpha_0) + \omega_1 - \frac{1}{h}(\dot{l}_{12}\sin\theta_{v_2} - \\ & \quad \dot{\varphi}_{12} l_{12}\cos\theta_{v_2}) \end{aligned} \quad (7)$$

where the amplitude A_θ and the phase α_0 are defined as $A_\theta = \sqrt{(k_A)^2 + (k_B)^2}$ and $\alpha_0 = \arctan(k_B/k_A)$ for $k_A = (v_1 - \omega_1 l_{12}\sin\varphi_{12})/h$ and $k_B = \omega_1 l_{12}\cos\varphi_{12}/h$, respectively.

Let $\boldsymbol{q}_d = (l_{12}^d \quad \varphi_{12}^d)^{\mathrm{T}}$ and $\dot{\boldsymbol{q}}_d = (\dot{l}_{12}^d \quad \dot{\varphi}_{12}^d)^{\mathrm{T}}$ be the desired relative formation motion states between two robots. Then, the formation tracking errors are represented by

$$\tilde{\boldsymbol{q}} = (l_{12} - l_{12}^d \quad \varphi_{12} - \varphi_{12}^d)^{\mathrm{T}},\ \dot{\tilde{\boldsymbol{q}}} = (\dot{l}_{12} - \dot{l}_{12}^d \quad \dot{\varphi}_{12} - \dot{\varphi}_{12}^d)^{\mathrm{T}}$$

The zero dynamics of the leader-follower robots system can be obtained by constraining all the tracking errors to zero and assuming $\dot{l}_{12}^d$ and $\dot{\varphi}_{12}^d$ to be zero. Physically, this means that the robots in formation are both keeping desired relative positions and moving at a constant linear velocity and angular velocity in the plane.

The zero dynamics[20] is given by

$$\dot{\theta}_{12} = -A_{\theta_0}\sin(\theta_{12} - \alpha_0) + \omega_1 \quad (8)$$

To make system (8) to have a stable equilibrium in the region $|\theta_{12} - \alpha_0| \le \pi/2$, the following condition should be satisfied

$$A_{\theta_0} > \omega_1 \quad (9)$$

for any ω_1 and v_1. If $\omega_1 = 0$, the stable equilibrium of system (8) is located at the origin. If condition (9) is not satisfied, the sign of $\dot{\theta}_{12}$ will remain positive or negative when the robots are in the desired formation configuration. In this case, the value of θ_{12} will increase or decrease continuously all the time, which means that the zero dynamics is unstable.

Condition (9) ensures the stability of the zero dynamics by limiting the range of the leader′s motion and the class of the desired formation configuration. Once condition (9) is satisfied, the relative angular velocity will converge to zero when the tracking errors converge to zero. In the case where condition (9) is not established, the solutions of (7) imply a continuous relative rotation motion between robots, and the relative angular velocity of the motion is periodically varying.

Assumption 1. For the velocity $(v_1 \quad \omega_1)^{\mathrm{T}}$ of the leader robot, the following condition holds

$$A_{\theta_0} > \omega_1$$

in the region $\|(\tilde{\boldsymbol{q}} \quad \dot{\tilde{\boldsymbol{q}}})^{\mathrm{T}}\| \le Q$, where Q is strictly positive.

Assumption 1 can be viewed as a cooperation protocol between the leader and the follower robot, which provides a stability margin for the zero dynamics.

2.3 Reformulation of internal dynamics

Under Assumption 1, the internal dynamics is reformulated in terms of tracking errors in this section. Through reformulation, we derive a bound for the time derivative of the square of the internal tracking error. This result will be used to prove the stability of the closed-loop system in the following section.

When the formation system is in steady state, the internal dynamics is given by

$$\dot{\beta}_0 = -A_\theta \sin\beta_0 + \omega_1 - \frac{1}{h}(\dot{l}_{12}^d \sin\theta_{v_2} - \dot{\varphi}_{12}^d l_{12}^d \cos\theta_{v_2}) \quad (10)$$

where β_0 is the solution of the stable internal dynamics. Make the following state transformation

$$\tilde{\theta}_{12} = \theta_{12} - \alpha_0 - \beta_0$$

and set the function

$$\Gamma(\tilde{\theta}_{12}, \dot{\tilde{\boldsymbol{q}}}) = \frac{1}{h}\big[-\sin\theta_{v_2} \quad l_{12}\cos\theta_{v_2}\big]\dot{\tilde{\boldsymbol{q}}} \quad (11)$$

Subtract (7) from (10). Then the internal dynamics of system (2) can be rewritten as

$$\dot{\tilde{\theta}}_{12} = -A_\theta\big[\sin(\tilde{\theta}+\beta_0)-\sin\beta_0\big]+\Gamma(\tilde{\theta}_{12},\dot{\tilde{\boldsymbol{q}}}) \tag{12}$$

Lemma 1. If the states l_{12} and $\tilde{\theta}_{12}$ are bounded by $\|l_{12}\| \le L$ and $\|\tilde{\theta}_{12}\| \le \Theta$, where L and Θ are positive constants, the internal state in (12) satisfies the following inequality

$$\tilde{\theta}_{12}\dot{\tilde{\theta}}_{12} \le -\rho_\theta\|\tilde{\theta}_{12}\|^2+\rho_1\|\dot{\tilde{\boldsymbol{q}}}_1\|\|\tilde{\theta}_{12}\|+\rho_2\|\dot{\tilde{\boldsymbol{q}}}_2\|\|\tilde{\theta}_{12}\| \tag{13}$$

where $\rho_\theta = 2A_\theta/3\min\{\cos(\beta_0+0.5\tilde{\theta}_{12})\}$ for $|\beta_0+0.5\tilde{\theta}_{12}| < 0.5\pi$, $\rho_1 = 1/h$, and $\rho_2 = L/h$.

Proof. Lemma 1 can be directly proved as follows. Internal dynamics (12) can be rewritten as

$$\begin{aligned}\dot{\tilde{\theta}}_{12} =& -A_\theta\big[\sin(\tilde{\theta}_{12}+\beta_0)-\sin\beta_0\big]+\Gamma(\tilde{\theta}_{12},\dot{\tilde{\boldsymbol{q}}}) = \\ & 2A_\theta\cos(\beta_0+\frac{\tilde{\theta}_{12}}{2})\sin\frac{\tilde{\theta}_{12}}{2}+\Gamma(\tilde{\theta}_{12},\dot{\tilde{q}})\end{aligned} \tag{14}$$

Multiplying (14) by $\tilde{\theta}_{12}$, we get

$$\tilde{\theta}_{12}\dot{\tilde{\theta}}_{12} = -2A_\theta\cos(\beta_0+\frac{\tilde{\theta}_{12}}{2})\tilde{\theta}_{12}\sin\frac{\tilde{\theta}_{12}}{2}+\tilde{\theta}_{12}\Gamma(\tilde{\theta}_{12},\dot{\tilde{q}}) \tag{15}$$

where $\tilde{\theta}_{12}\sin(0.5\tilde{\theta}_{12}) \ge 0$ and $\big|\sin 0.5\tilde{\theta}_{12}\big| \ge \big|\tilde{\theta}_{12}\big|/3$ for $\big|\tilde{\theta}_{12}\big| \le 0.5\pi$, and

$$\begin{aligned}\tilde{\theta}_{12}\Gamma(\tilde{\theta}_{12},\dot{\tilde{\boldsymbol{q}}}) &= \frac{1}{h}\tilde{\theta}_{12}\big[-\sin\theta_{v_2}, l_{12}\cos\theta_{v_2}\big]\dot{\tilde{\boldsymbol{q}}} \\ &\le \frac{1}{h}\|\tilde{\theta}_{12}\|\|\dot{\tilde{\boldsymbol{q}}}_1\|+\frac{L}{h}\|\tilde{\theta}_{12}\|\|\dot{\tilde{\boldsymbol{q}}}_2\|\end{aligned}$$

Then, the following inequality holds

$$\tilde{\theta}_{12}\dot{\tilde{\theta}}_{12} < -\rho_\theta\|\tilde{\theta}_{12}\|^2+\frac{1}{h}\|\tilde{\theta}_{12}\|\|\dot{\tilde{\boldsymbol{q}}}_1\|+\frac{L}{h}\|\tilde{\theta}_{12}\|\|\dot{\tilde{\boldsymbol{q}}}_2\| \tag{16}$$

for $\rho_\theta = 2A_\theta/3\min\{\cos(\beta_0+0.5\tilde{\theta}_{12})\}$ and $\big|\tilde{\theta}_{12}\big| \le 0.5\pi$. Thus, Lemma 1 is proved. □

Lemma 1 shows that the internal dynamics becomes stable when the perturbation $\Gamma(\tilde{\theta}_{12},\dot{\tilde{\boldsymbol{q}}})$ vanishes at the origin. The stability can also be seen from (14). If the tracking error $(\tilde{\boldsymbol{q}} \quad \dot{\tilde{\boldsymbol{q}}})^{\mathrm{T}}$ converges so that the following inequality is satisfied,

$$\Big|2A_\theta\cos(\beta_0+\frac{\tilde{\theta}_{12}}{2})\Big| \ge \big|\Gamma(\tilde{\theta}_{12},\dot{\tilde{\boldsymbol{q}}})\big| \tag{17}$$

then the internal tracking error $\tilde{\theta}_{12}$ approaches zero. An effective method to stabilize internal dynamics (14) is to force the tracking error $(\tilde{\boldsymbol{q}} \quad \dot{\tilde{\boldsymbol{q}}})^{\mathrm{T}}$ approach origin sufficiently fast to satisfy (17) for system (5), which will be discussed in the following section.

3 Robust formation control

In this section, a robust controller is designed to stabilize the system in the presence of modeling uncertainty. The objective is to develop a control law to determine $\boldsymbol{u} = (\dot{v}_2 \quad \dot{\omega}_2)^{\mathrm{T}}$ for the leader-follower formation system such that the follower robot tracks the leader robot with a given formation configuration $\boldsymbol{q}_d = (l_{12}^d \quad \varphi_{12}^d)^{\mathrm{T}}$.

The proposed control scheme consists of a nominal part designed based on the nominal model of the system without the perturbation of modeling uncertainty and a sliding mode robust compensator to stabilize the overall system in the presence of uncertainty. The overall control is defined as

$$\boldsymbol{u} = \underbrace{M\ddot{\boldsymbol{q}}_r+C\dot{\boldsymbol{q}}+G}_{u_0}-\underbrace{M\boldsymbol{\eta}\,\mathrm{sgn}(s)}_{u_1} \tag{18}$$

where u_0 is the nominal control, and u_1 is a sliding mode compensator. Their design is described in the following. The new reference acceleration vector $\ddot{\boldsymbol{q}}_r$ is formed by shifting the desired acceleration $\ddot{\boldsymbol{q}}_d$ according to the position error $\tilde{\boldsymbol{q}}$ and velocity error $\dot{\tilde{\boldsymbol{q}}}$.

$$\ddot{\boldsymbol{q}}_r = \ddot{\boldsymbol{q}}_d-\Lambda_2\dot{\tilde{\boldsymbol{q}}}-\Lambda_1\tilde{\boldsymbol{q}} \tag{19}$$

where $\Lambda_i = \mathrm{diag}(\lambda_{i1} \quad \lambda_{i2})$ for $i = 1, 2$ are symmetric positive definite matrices. Thus, the reference trajectory is expressed in terms of the tracking errors. The component of the constant vector $\boldsymbol{\eta}$ satisfy $\eta_i > [|M^{-1}\boldsymbol{\delta}|]_i+\eta_{0i}$, where η_{0i} is a strictly positive constant.

The nominal control u_0 in (18) leads to a linear closed-loop equation of the nominal system

$$\ddot{\tilde{\boldsymbol{q}}} = -\Lambda_2\dot{\tilde{\boldsymbol{q}}}-\Lambda_1\tilde{\boldsymbol{q}} \tag{20}$$

and control law (18) results in the actual closed-loop system of (5) in the form of

$$\ddot{\boldsymbol{q}} = \ddot{\boldsymbol{q}}_r-\boldsymbol{\eta}\,\mathrm{sgn}(s)-M^{-1}\boldsymbol{\delta} \tag{21}$$

Define the tracking errors as $\boldsymbol{z}_i = \big[\tilde{\boldsymbol{q}}_i \quad \dot{\tilde{\boldsymbol{q}}}_i\big]^{\mathrm{T}}$ for $i = 1, 2$ and $\tilde{\theta}_{12} = (\theta_{12}-\alpha_0)-\beta_0$ where β_0 is the stable solution of zero dynamics (8) under Assumption 1. Then, the closed-loop equation can be written as

$$\begin{aligned}\begin{bmatrix}\dot{z}_1\\ \dot{z}_2\end{bmatrix} &= \begin{bmatrix}A_1 & 0\\ 0 & A_2\end{bmatrix}\begin{bmatrix}z_1\\ z_2\end{bmatrix}- \\ &\quad \begin{bmatrix}0\\ [\boldsymbol{\eta}\,\mathrm{sgn}(s)+M^{-1}\boldsymbol{\delta}]_1\\ 0\\ [\boldsymbol{\eta}\,\mathrm{sgn}(s)+M^{-1}\boldsymbol{\delta}]_2\end{bmatrix}\end{aligned} \tag{22a}$$

$$\dot{\tilde{\theta}}_{12} = -2k_\theta\cos(\beta_0+\frac{\tilde{\theta}_{12}}{2})\sin(\frac{\tilde{\theta}_{12}}{2})+\Gamma(\tilde{\theta}_{12},\dot{\tilde{\boldsymbol{q}}}) \tag{22b}$$

where

$$A_i = \begin{pmatrix}0 & 1\\ -\lambda_{i1} & -\lambda_{i2}\end{pmatrix}, \quad i = 1, 2$$

Let P_i be the symmetric positive definite solution of the following Lyapunov equation

$$A_i^{\mathrm{T}}P_i+P_iA_i = -Q_i, \quad i = 1, 2 \tag{23}$$

where Q_1 and Q_2 are symmetric positive definite matrices. Let $\lambda_{\min}(Q_i)$ denote the smallest eigenvalue of the matrix Q_i. The stability of the resultant closed-loop (22) can be proved using the Lyapunov theory.

Theorem 1. If Assumption 1 holds, closed-loop system (22) under control law (18) is asymptotically stable at the origin with the variable s_i in (18) selected as

$$\boldsymbol{s}_i = [\boldsymbol{z}_i^{\mathrm{T}}P_i]_2, \qquad i = 1, 2 \tag{24}$$

where $[\boldsymbol{z}_i^{\mathrm{T}} P_i]_2$ denotes the second element of the vector $\boldsymbol{z}_i^{\mathrm{T}} P_i$, and Λ_1 and Λ_2 are designed such that the following inequality holds

$$2\lambda_{\min}(Q_i)\ \rho_\theta - \rho_i^2 > 0, \qquad i = 1, 2 \tag{25}$$

Proof. Consider the composite Lyapunov function candidate

$$V(t) = \frac{1}{2}\sum_{i=1}^{2} \boldsymbol{z}_i^{\mathrm{T}} P_i \boldsymbol{z}_i + \frac{1}{2}\tilde{\boldsymbol{\theta}}^{\mathrm{T}}\tilde{\boldsymbol{\theta}} \tag{26}$$

Differentiating (26) with time along the solutions of (22), substituting $\boldsymbol{z}_i^{\mathrm{T}} P_i$ with s_i from (24), and using inequality (13), we have

$$\begin{aligned}
\dot{V}(t) &= \frac{1}{2}\sum_{i=1}^{2}(\dot{\boldsymbol{z}}_i^{\mathrm{T}} P_i \boldsymbol{z}_i + \boldsymbol{z}_i^{\mathrm{T}} P_i \dot{\boldsymbol{z}}_i) + \tilde{\theta}^{\mathrm{T}}\dot{\tilde{\theta}} = \\
&\sum_{i=1}^{2}\Big\{ -\frac{1}{2}\boldsymbol{z}_i^{\mathrm{T}} Q_i \boldsymbol{z}_i - \\
&\boldsymbol{z}_i^{\mathrm{T}} P_i \begin{bmatrix} 0 \\ \eta_i \operatorname{sgn}(s_i) + (M^{-1}\boldsymbol{\delta})_i \end{bmatrix}\Big\} + \tilde{\theta}^{\mathrm{T}}\dot{\tilde{\theta}} \le \\
&-0.5\sum_{i=1}^{2}\lambda_{\min}(Q_i)\big\|\boldsymbol{z}_i\big\|^2 - \rho_\theta\big\|\tilde{\theta}_{12}\big\|^2 + \\
&\sum_{i=1}^{2}\rho_i\big\|\boldsymbol{z}_i\big\|\big\|\tilde{\theta}_{12}\big\| - \sum_{i=1}^{2}\eta_{0i}|s_i| = \\
&-\sum_{i=1}^{2}\begin{bmatrix}\|\boldsymbol{z}_i\| & \|\tilde{\theta}_{12}\|\end{bmatrix}\cdot\begin{bmatrix} 0.5\lambda_{\min}(Q_i) & -0.5\rho_i \\ -0.5\rho_i & 0.5\rho_\theta \end{bmatrix}\cdot \\
&\begin{bmatrix} \|\boldsymbol{z}_i\| \\ \|\tilde{\theta}_{12}\| \end{bmatrix} - \sum_{i=1}^{2}\eta_{0i}|s_i|
\end{aligned} \tag{27}$$

From the last equation of (27), we have $\dot{V}(t) < 0$ provided that $\lambda_{\min}(Q_i)\rho_\theta - \rho_i^2 > 0$ for $i = 1, 2$, and $(\boldsymbol{z}_1 \quad \boldsymbol{z}_2 \quad \tilde{\theta}_{12}) \neq 0$. Thus, Theorem 1 is proved. □

The stability of the closed-loop system is guaranteed through the design of feedback gains in u_0, which satisfies robustness inequality (25) by solving Lyapunov equation (23). In (27), the perturbation from the internal dynamics is suppressed by decreasing formation tracking errors. Thus, even the internal dynamics is not in its stable region, the whole closed-loop system is still stable. The proper selection of the control gains in u_0 makes the whole system robust to the internal perturbations.

The gain ρ_θ in (25) is determined by the configuration of the formation. As it can be noted, a larger ρ_θ leads to a smaller $\lambda_{\min}(Q_i)$, equivalently, a lower gain of the controller. Thus, robustness inequality (25) provides a tradeoff between the feedback gains and the nature of formation commands that can be tracked. The control chattering introduced by the switching term u_1 can be treated using a saturation function such as the one described in [23].

4 Robust adaptive formation control

In Section 3, we made an assumption that the parameter h of the follower robot is exactly known. However, the rotation center of a mobile robot in practice is not strictly on the axis of symmetry as in theory, which is due to the error of machining and installation of robot wheels. On the other hand, it is difficult to measure the actual rotation center when the mobile robot is in motion. In addition, the calibration error of visual measurement system can also cause uncertainty in determining the value of h. Thus, the accurate value of h may be unavailable under certain situations.

In this section, we take the uncertainty in h into account and propose an adaptive control method to improve the control performance. Inspired by [21] and [22], we rewrite the nominal part of controller (18) in a decomposed form: an uncertainty free part denoted by u_{NA} and the second part contains the parameter uncertainty and is written in a form of vector product described by $Y_{2\times 2}H_{2\times 1}$, as shown in the following equation.

$$\begin{aligned}
\begin{pmatrix} \dot{v}_2 \\ \dot{\omega}_2 \end{pmatrix} &= M\left\{\begin{pmatrix} \ddot{l}_{12}^r \\ \ddot{\varphi}_{12}^r \end{pmatrix} + \begin{pmatrix} -l_{12}\dot{\varphi}_{12} \\ \dot{l}_{12}/l_{12} \end{pmatrix}\omega_2\right\} + \\
&C\begin{pmatrix} \dot{l}_{12} \\ \dot{\varphi}_{12} \end{pmatrix} - \dot{\theta}_{12}\begin{pmatrix} d\omega_2 \\ -v_2/d \end{pmatrix} = \\
&\boldsymbol{u}_{NA} + Y_{2\times 2}H_{2\times 1}
\end{aligned} \tag{28}$$

where

$$\boldsymbol{u}_{NA} = \begin{bmatrix} u_{n0} \\ 0 \end{bmatrix},\ Y = \begin{bmatrix} -\omega_2\dot{\theta}_{12} & 0 \\ 0 & y_{22} \end{bmatrix},\ \boldsymbol{H} = \begin{bmatrix} h \\ 1/h \end{bmatrix},$$

where

$$\begin{aligned}
u_{n0} &= -(\ddot{l}_{12}^r + \dot{\varphi}_{12}l_{12}(\dot{\varphi}_{12} + \dot{\theta}_{12} - \omega_2))\cos\theta_{v_2} - \\
&\quad (\ddot{\varphi}_{12}^r l_{12} + \dot{l}_{12}(2\dot{\varphi}_{12} + \dot{\theta}_{12} - \omega_2))\sin\theta_{v_2} \\
y_{22} &= (\ddot{l}_{12}^r - \dot{\varphi}_{12}l_{12}(\dot{\varphi}_{12} + \dot{\theta}_{12} + \omega_2))\sin\theta_{v_2} + v_2\dot{\theta}_{12} - \\
&\quad (\ddot{\varphi}_{12}^r l_{12} + \dot{l}_{12}(2\dot{\varphi}_{12} + \dot{\theta}_{12} + \omega_2))\cos\theta_{v_2}
\end{aligned}$$

and $\ddot{\boldsymbol{q}}_r = \ddot{\boldsymbol{q}}_d - \Lambda_2\dot{\tilde{\boldsymbol{q}}} - \Lambda_1\tilde{\boldsymbol{q}}$.

The vector $\ddot{\boldsymbol{q}}_r$ is the same as defined in (19). The vector $\boldsymbol{H}$ contains the parameters to be estimated by an adaptive estimation algorithm. In the following, the vector $\hat{\boldsymbol{H}}$ will be used to denote the estimation of $\boldsymbol{H}$, and the estimation error is presented by the vector $\tilde{\boldsymbol{H}} = \boldsymbol{H} - \hat{\boldsymbol{H}}$. Similarly, the estimation error of the matrix M is given by

$$\begin{aligned}
\tilde{M} &= M - \hat{M} = \\
&\frac{(\hat{h} - h)}{h\hat{h}}\begin{pmatrix} 0 & 0 \\ \sin\theta_{v_2} & -l_{12}\cos\theta_{v_2} \end{pmatrix}
\end{aligned} \tag{29}$$

where $\hat{M}$ is the estimation of the matrix M. Clearly, if $\hat{h} = h$, we have $\tilde{M} = 0$. The uncertainty of $\tilde{M}$ is only associated with the estimation error of h or, equivalently, H.

Now, take the uncertainty of $\boldsymbol{H}$ into account and revise (28) in the form of

$$\begin{aligned}
\hat{u} &= \hat{M}\ddot{\boldsymbol{q}}_r + \hat{C}\dot{\boldsymbol{q}} + \hat{G} = \\
&\boldsymbol{u}_{NA} + Y_{2\times 2}\hat{\boldsymbol{H}}_{2\times 1}
\end{aligned} \tag{30}$$

where the matrixes $\hat{C}$ and $\hat{G}$ denote the estimations of C and G, respectively. (30) is the controller for nominal part of system (2) when the system suffers from the parameter uncertainty of h.

Based on the above discussion, a robust adaptive controller for the leader-follower robots system can be designed as

$$\boldsymbol{u} = \boldsymbol{u}_{NA} + Y\hat{\boldsymbol{H}} - \hat{M}\boldsymbol{\eta}\operatorname{sgn}(s) \tag{31a}$$

$$\dot{\hat{\boldsymbol{H}}} = -\Gamma(\hat{M}^{-1}Y)^{\mathrm{T}}\begin{bmatrix}[\boldsymbol{z}_1^{\mathrm{T}}P_1]_2\\ [\boldsymbol{z}_2^{\mathrm{T}}P_2]_2\end{bmatrix} \tag{31b}$$

where Γ is a symmetric positive definite matrix, and a constant η_i is chosen such that the following inequalities hold true

$$\eta_i > |[\hat{M}^{-1}(\tilde{M}\ddot{\boldsymbol{q}}+\boldsymbol{\delta})]_i| + \eta_{0i}, \qquad i=1,2 \tag{32}$$

where η_{01} and η_{02} are positive constants and $\ddot{\tilde{\boldsymbol{q}}} = \ddot{\boldsymbol{q}}_r - \ddot{\boldsymbol{q}}$, and $s_i = [\boldsymbol{z}_i^{\mathrm{T}}P_i]_2$ for $i=1,2$.

Controller (31) is composed of two parts: the first part is the output equation of the dynamical controller system, which has the same structure as control law (18) in Section 3 and provides the control action to the follower robot; the second part is the dynamical part, which adaptively estimates the vector $\boldsymbol{H}$ needed by the first part.

The resulting closed-loop system using control law (31) is given by

$$\begin{bmatrix}\dot{\boldsymbol{z}}_1\\ \dot{\boldsymbol{z}}_2\end{bmatrix} = \begin{bmatrix}A_1 & 0\\ 0 & A_2\end{bmatrix}\begin{bmatrix}\boldsymbol{z}_1\\ \boldsymbol{z}_2\end{bmatrix} - \begin{bmatrix}0\\ [\hat{M}_1Y\tilde{H}]_1+\eta_1\,\mathrm{sgn}(s_1)+[\hat{M}^{-1}(\tilde{M}\ddot{\boldsymbol{q}}+\boldsymbol{\delta})]_1\\ 0\\ [\hat{M}_1Y\tilde{H}]_2+\eta_2\,\mathrm{sgn}(s_2)+[\hat{M}^{-1}(\tilde{M}\ddot{\boldsymbol{q}}+\boldsymbol{\delta})]_2\end{bmatrix} \tag{33a}$$

$$\dot{\tilde{\theta}}_{12} = -2k_\theta\cos(\beta_0+\frac{\tilde{\theta}_{12}}{2})\sin\frac{\tilde{\theta}_{12}}{2} + \Gamma(\tilde{\theta}_{12},\dot{\tilde{\boldsymbol{q}}}) \tag{33b}$$

The stability of closed-loop system (33) is proved by the Lyapunov theory in the following.

Theorem 2. If Assumption 1 holds, the closed-loop system (33) under controller (31) is asymptotically stable at the origin, provided that the variable s_i in (31a) is set at $s_i = [\boldsymbol{z}_i^{\mathrm{T}}P_i]_2$ for $i=1,2$, and Λ_1 and Λ_2 are chosen such that inequality (25) holds.

Proof. Select the Lyapunov function candidate

$$V(t) = \frac{1}{2}(\sum_{i=1}^{2}\boldsymbol{z}_i^{\mathrm{T}}P_i\boldsymbol{z}_i + \tilde{\boldsymbol{\theta}}^{\mathrm{T}}\tilde{\boldsymbol{\theta}} + \tilde{\boldsymbol{H}}^{\mathrm{T}}\Gamma^{-1}\tilde{\boldsymbol{H}}) \tag{34}$$

Differentiating (34) with respect to time along the solutions of system (33), we have

$$\begin{aligned}\dot{V}(t) = {} & \frac{1}{2}\sum_{i=1}^{2}(\dot{\boldsymbol{z}}_i^{\mathrm{T}}P_i\boldsymbol{z}_i + \boldsymbol{z}_i^{\mathrm{T}}P_i\dot{\boldsymbol{z}}_i) + \tilde{\boldsymbol{\theta}}^{\mathrm{T}}\dot{\tilde{\boldsymbol{\theta}}} + \dot{\tilde{\boldsymbol{H}}}^{\mathrm{T}}\Gamma^{-1}\tilde{\boldsymbol{H}} = \\ & \sum_{i=1}^{2}\Big\{-\frac{1}{2}\boldsymbol{z}_i^{\mathrm{T}}Q_i\boldsymbol{z}_i - \\ & \boldsymbol{z}_i^{\mathrm{T}}P_i\begin{bmatrix}0\\ \eta_i\,\mathrm{sgn}(s_i)+[\hat{M}^{-1}(\tilde{M}\ddot{\boldsymbol{q}}+\boldsymbol{\delta})]_i\end{bmatrix}\Big\} - \\ & \begin{bmatrix}[\boldsymbol{z}_1^{\mathrm{T}}P_1]_2\\ [\boldsymbol{z}_2^{\mathrm{T}}P_2]_2\end{bmatrix}^{\mathrm{T}}\hat{M}^{-1}Y\tilde{\boldsymbol{H}} + \tilde{\boldsymbol{\theta}}^{\mathrm{T}}\dot{\tilde{\boldsymbol{\theta}}} + \dot{\tilde{\boldsymbol{H}}}^{\mathrm{T}}\Gamma^{-1}\tilde{\boldsymbol{H}}\end{aligned} \tag{35}$$

Using inequalities (13) and (25) to (35), and substituting $\dot{\tilde{\boldsymbol{H}}}$ from (31b), we get

$$\begin{aligned}\dot{V}(t) \le {} & -\sum_{i=1}^{2}0.5\lambda_{\min}(Q_i)\|\boldsymbol{z}_i\|^2 - \rho_\theta\|\tilde{\theta}_{12}\|^2 + \\ & \sum_{i=1}^{2}\rho_i\|\boldsymbol{z}_i\|\|\tilde{\theta}_{12}\| - \sum_{i=1}^{2}\eta_{0i}|s_i| - \\ & \sum_{i=1}^{2}[\boldsymbol{z}_i^{\mathrm{T}}P_i]_2[\hat{M}^{-1}Y\tilde{H}]_i + \dot{\tilde{\boldsymbol{H}}}^{\mathrm{T}}\Gamma^{-1}\tilde{\boldsymbol{H}} = \\ & -\sum_{i=1}^{2}[\|\boldsymbol{z}_i\|\ \|\tilde{\theta}_{12}\|]\cdot\begin{bmatrix}0.5\lambda_{\min}(Q_i) & -0.5\rho_i\\ -0.5\rho_i & 0.5\rho_\theta\end{bmatrix}\cdot \\ & \begin{bmatrix}\|\boldsymbol{z}_i\|\\ \|\tilde{\theta}_{12}\|\end{bmatrix} - \sum_{i=1}^{2}\eta_{0i}|s_i|\end{aligned} \tag{36}$$

From (36), we have $\dot{V}(t) < 0$ provided that $\lambda_{\min}(Q_i)\rho_\theta - \rho_i^2 > 0$ for $i=1,2$, and $(\boldsymbol{z}_1 \quad \boldsymbol{z}_2 \quad \tilde{\theta}_{12})^{\mathrm{T}} \neq 0$. Thus, Theorem 2 is proved. □

Under the adaptive control law, the effect from the uncertainty of parameter h has been compensated. As a result, the amplitude of switching term in (31a) will increase due to the term $\tilde{M}\ddot{\boldsymbol{q}}$ in (32).

5 Simulations

We will now illustrate the effectiveness of the proposed control schemes by studying the following examples. The formation configuration is defined as

$$\boldsymbol{q}_d = (l_{12}^d \quad \varphi_{12}^d)^{\mathrm{T}} = (400 \quad 2\pi/3)^{\mathrm{T}}$$

The actual value of parameter h in the simulations is set at $h = 100\,\mathrm{mm}$. The trajectory of the leader robot is defined by an ellipse curve in the first phase, and then the trajectory is defined by a circle after point A, as depicted in Fig. 2. The trajectory of the leader robot is smooth with uniform linear and angular velocities and accelerations except for point A.

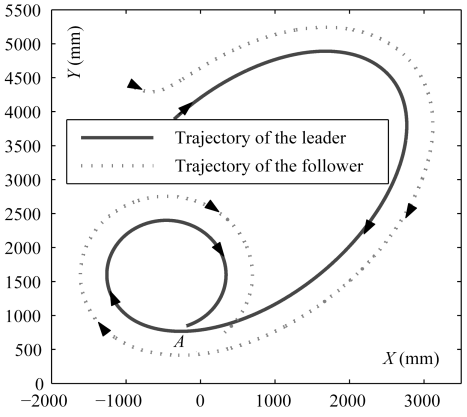

Fig. 2 The trajectories of the two robots

The control parameters are selected as

$$\lambda_{11} = \lambda_{21} = 30, \quad \lambda_{12} = \lambda_{22} = 20, \quad \eta_1 = 15, \quad \eta_2 = 0.06$$

By solving the Lyapunov function $A_i^{\mathrm{T}}P_i + P_iA_i = -I$, the

matrixes P_1 and P_2 are given by

$$P_1 = P_2 = \begin{pmatrix} 0.3592 & -0.5 \\ -0.5 & 0.7750 \end{pmatrix}$$

Then, the sliding variables in (18) are determined as

$$\begin{aligned} s_1 &= [\boldsymbol{z}_1^{\mathrm{T}} P_1]_2 = -0.5(l_{12} - l_{12}^d) + 0.7750\,\dot{l}_{12} \\ s_2 &= [\boldsymbol{z}_2^{\mathrm{T}} P_2]_2 = -0.5(\varphi_{12} - \varphi_{12}^d) + 0.7750\,\dot{\varphi}_{12} \end{aligned}$$

Under controller (18), the trajectories of the two robots are depicted in Fig. 2. In the presence of initial formation tracking errors, the formation states are shown in Fig. 3. Both the relative distance and the relative bearing converge to their desired values, and the relative orientation remains bounded in the whole process. At point A, the motion mode of the leader robot switches from the ellipse cure to a circle, and at the same time, the relative orientation increases to a new steady state to adapt to the new motion mode of the leader robot.

The corresponding acceleration commands are shown in Fig. 4. Both of the commanded accelerations approach zero when the robots converge to the desired configuration. The peaks appearing on the curves at 45th second are due to the disturbance from the discontinuous motion of the leader robot at point A. In implementation, the acceleration inputs are translated into velocity variations by multiplying them with the control period. Hence, the reference velocities for the follower robot can be obtained by adding the velocity variations to the current velocity.

Adaptive robust controller (31) is also tested. The control parameters are chosen as

$$\lambda_{11} = \lambda_{21} = 30, \quad \lambda_{12} = \lambda_{22} = 20, \quad \eta_1 = 16, \quad \eta_2 = 0.08$$

By comparative simulation tests, the gain for the adaptive estimator is designed as

$$\Gamma = \mathrm{diag}\,(\tau_1 \quad \tau_2) = \mathrm{diag}\,(1 \quad 0.002)$$

It should be noted that high estimator gain will make the estimator excessively sensitive to the system tracking errors. For instance, high value of τ_2 will introduce control chattering into the commanded angular acceleration of the follower robot.

The initial estimate of parameter h is set at $\hat{h} = 150\,\mathrm{mm}$, whereas its actual value is 100 mm. To show the effectiveness of the proposed controller under the parametric uncertainty in h, here, we make the initial error as large as 50 %. In practice, the initial estimation error may be likely smaller than 50 %.

Under controller (31), the trajectories of the two robots are depicted in Fig. 5. To test the proposed approach in a more rigorous situation, the trajectory of the leader robot is defined by a more complex curve composed of several ellipse and circle curves. The distance from the starting point of the follower robot to the leader robot is also larger than the corresponding distance in the first test.

The corresponding formation states are shown in Fig. 6. Both the relative distance and the relative bearing converge to their desired values, and the parametric uncertainty in h is effectively compensated by the adaptive controller. In contrast to Fig. 3, more severe oscillation appears in the internal state curve, but the oscillation has little impact on the formation tracking errors, as shown in Fig. 6. This shows that the formation system is robust to the perturbation from that the internal dynamics.

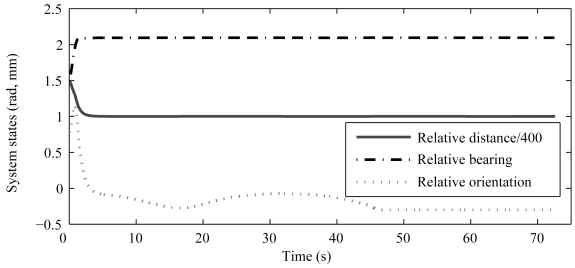

Fig. 3 The formation states

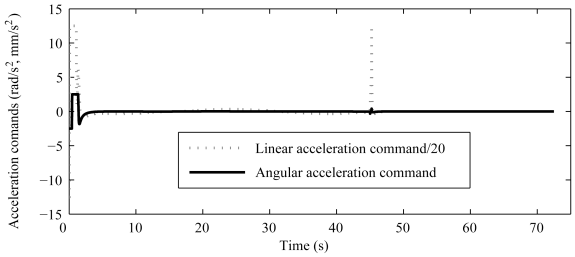

Fig. 4 The commanded linear and angular accelerations

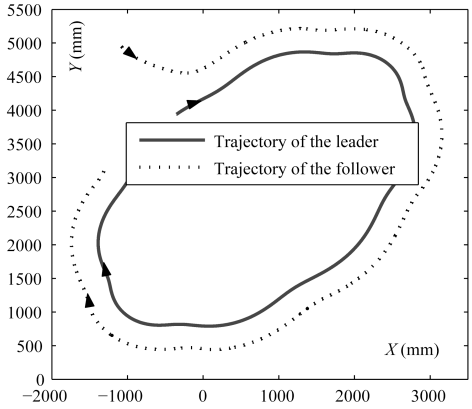

Fig. 5 The trajectories of the two robots by using adaptive controller (31)

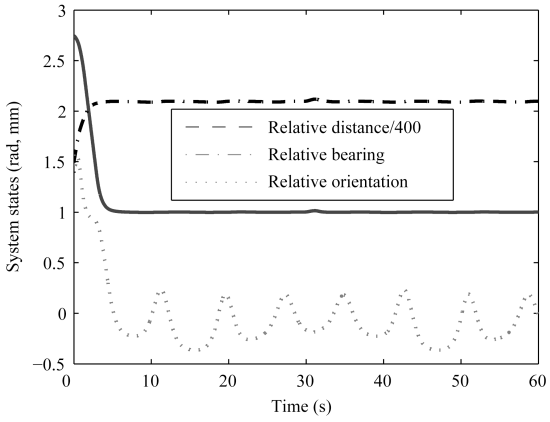

Fig. 6 The system states by using adaptive controller (31)

The values of $\dot{\theta}_{12}$ and $\dot{\theta}_{v_2}$ are shown in Fig. 7. After the initial phase, they have the same amplitudes but with opposite signs, and this verifies that $\dot{\varphi}_{12}$ approaches zero on

one side since $\dot{\theta}_{v_2} = -\dot{\varphi}_{12} - \dot{\theta}_{12}$. The estimation of parameter vector $\boldsymbol{H} = [h_1, h_2]^{\mathrm{T}}$ is shown in Fig. 8. Although the estimates of h_1 and h_2 do not converge to their actual values, the tracking formation errors still approach zero, as shown in Fig. 6, and an explanation for this phenomenon can be found in [17]. The output accelerations of the controller (18) are depicted in Fig. 9. When the leader robot moves along the irregular trajectory shown in Fig. 5, the follower robot continually regulates its commanded accelerations to track the leader robot with desired formation. After the initial phase, the commanded linear acceleration varies approximately with a fixed period to adapt to the motion of the leader robot.

6 Experiments

Experimental investigation has been conducted using three nonholonomic mobile robots, as shown in Fig. 10. A vision system transplanted from a robot-soccer platform is used to measure the relative positions between mobile robots. The vision system recognizes each robot by the color marker adhibited on the top of each robot, as shown in Fig. 10. A virtual vision sensor is fixed on each follower robot. The virtual sensor translates the relative positions obtained by the actual vision system into the relative motion states from the view of the follower robot.

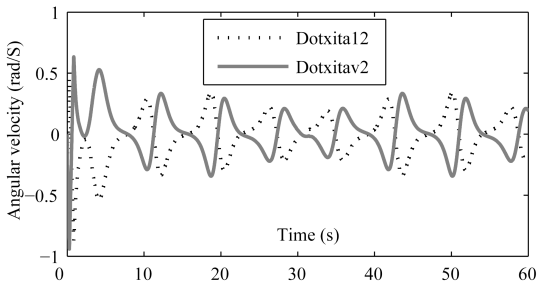

Fig. 7 The derivatives of angular θ_{12} and angular θ_{v_2} by using adaptive controller (31)

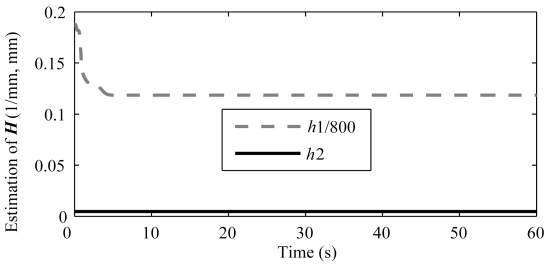

Fig. 8 The estimation of $\boldsymbol{H}$ by using adaptive controller (31)

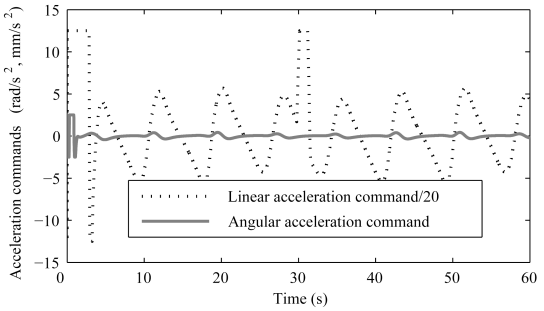

Fig. 9 The commanded linear and angular accelerations

Fig. 10 Three robots formation moving

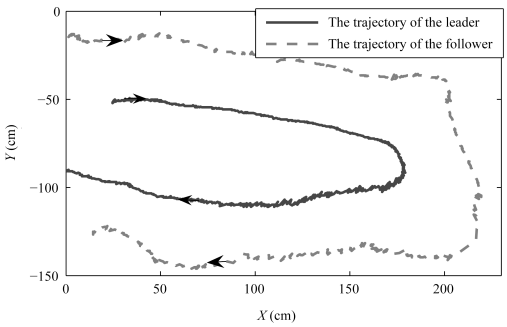

Fig. 11 (a) The trajectories of the leader robot R_1 and the follower robot R_2

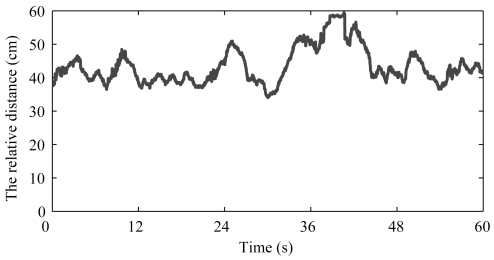

Fig. 11 (b) The relative distance between robot R_1 and robot R_2

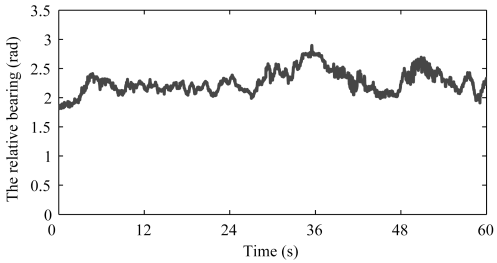

Fig. 11 (c) The relative bearing between robot R_1 and robot R_2

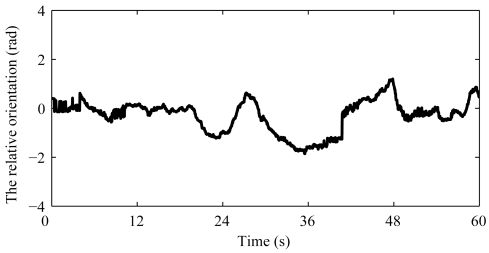

Fig. 11 (d) The relative orientation between robot R_1 and robot R_2

The leader robot in the group is controlled by a joystick and runs an arbitrary trajectory, as shown in Fig. 11(a). Each follower robot in the group is controlled by decentralized leader-follower controller (18) with the desired configuration $\boldsymbol{q}_d = (l_{12}^d \quad \varphi_{12}^d)^{\mathrm{T}} = (40\mathrm{cm} \quad 2\pi/3)^{\mathrm{T}}$. Under the proposed formation controller (18), the trajectories of the two follower robots, as recorded by the vision system, are depicted in Fig. 11(a). The corresponding formation states are shown in Fig. 11(b) and Fig. 11(c). Both of the tracking errors are limited when the formation is in the steady state. When the trajectory of the leader robot is not smooth, the rotation motion of the leader robot varies with high frequency. As a result, the perturbations from the internal dynamics becomes larger, as shown in Fig. 11(d). As depicted in Fig. 11(b) and Fig. 11(c), in this stage, both of the formation tracking errors remain bounded and are influenced little by the varying of internal state, showing that the formation system is robust to the perturbation from the internal dynamics.

7 Conclusions

In this paper, we have derived a second order kinematics model for leader-follower formation of mobile robots. Based on this model, a robust controller is proposed to control the leader-follower formation using only the relative measurement of the motion states between robots. The proposed controller does not need global sensor for formation control, and makes the closed-loop formation system robust to the perturbations from internal dynamics and the uncertainty associated with the absolute acceleration of the leader robot. Furthermore, a robust adaptive controller is developed, as an upgrading version of the robust controller, to deal with the parameter uncertainty associated with the rotation center of the follower robots. Simulation and experimental results have demonstrated the effectiveness of the proposed methods.

References

1 Desai J P, Ostrowski J, Kumar V. Controlling formations of multiple mobile robots. In: Proceedings of 1998 IEEE International Conference on Robotics and Automation. IEEE, 1998. 2864∼2869

2 Desai J P, Ostrowski J, Kumar V. Modeling and control of formations of nonholonomic mobile robots. *IEEE Transactions on Robotics and Automation*, 2001, **17**(6): 905∼908

3 Das K, Fierro R, Kumar V, Ostrowski J P, Spletzer J, Taylor C J. A vision-based formation control framework. *IEEE Transactions on Robotics and Automation*, 2002, **18**(5): 813∼825

4 Vidal R, Shakernia O, Sastry S. Distributed formation control with omnidirectional vision-based motion segmentation and visual servoing. *IEEE Robotics & Automation Magazine*, 2004, **11**(14): 14∼20

5 Ogren P, Egerstedt M, Hu X. A control Lyapunov function approach to multi-agent coordination. *IEEE Transactions on Robotics and Automation*, 2002, **18**(5): 847∼851

6 Egerstedt M, Hu X, Stotsky A. Control of mobile platforms using a virtual vehicle approach. *IEEE Transactions on Automatic Control*, 2001, **46**(11): 1777∼1782

7 Balch T, Arkin R C. Behavior-based formation control for multirobot teams. *IEEE Transactions on Robotics and Automation*, 1998, **14**(6): 926∼939

8 Parker L E. ALLIANCE: an architecture for fault tolerant multirobot cooperation. *IEEE Transactions on Robotics and Automation*, 1998, **14**(2): 220∼240

9 Fredslund J, Mataric M J. A general algorithm for robot formations using local sensing and minimal communication. *IEEE Transactions on Robotics and Automation*, 2002, **18**(5): 837∼846

10 Lawton J R T, Beard R W, Young B J. A decentralized approach to formation maneuvers. *IEEE Transactions on Robotics and Automation*, 2003, **19**(6): 933∼941

11 Jadbabaie A, Lin J, Morse A S. Coordination of groups of mobile autonomous agents using nearest neighbor rules. *IEEE Transactionss on Automatic Control*, 2002, **48**(6): 988∼1001

12 Tanner H G, Jadbabaie A, Pappas G J. Flocking in teams of nonholonomic agents. *Lecture Notes in Control and Information Sciences*. Berlin: Springer-Verlag, 2005. 229∼239

13 Reynolds C. Flocks, birds, and schools: a distributed behavioral model. *Computer Graphics*, 1987, **21**(4): 25∼34

14 Warburton K, Lazarus J. Tendency-distance models of social cohesion in animal groups. *Journal of Theoretical Biology*, 1991, **150**(4): 473∼488

15 Vidal R, Shakernia O, Sastry S. Omnidirectional vision-based formation control. In: Proceedings of the Allerton Conference on Communication, Control, and Computing. Monticello, Italy, 2002. 1625∼1634

16 Chiem S Y, Cervera E. Vision-based robot formations with Bezier trajectories. In: Proceedings of Intelligent Autonomous Systems. Amsterdam: IOS Press, 2004. 191∼198

17 Wesselowski K, Fierro R. A dual-mode model predictive controller for robot formations. In: Proceedings of the IEEE 2003 Conference on Decision and Control. IEEE, 2003. 3615∼3620

18 Sanchez J, Fierro R. Sliding mode control for robot formations. In: Proceedings of the 2003 IEEE International Symposium on Intelligent Control. IEEE, 2003. 438∼443

19 Orqueda O A A, Fierro R. Robust vision-based nonlinear formation control. In: Proceedings of the 2006 American Control Conference. Minneapolis, IEEE, 2006. 14∼16

20 Isidori A. *Nonlinear Control Systems: An Introduction*. New York: Springer-Verlag, 1989

21 Liu G, Goldenberg A A. Uncertainty decomposition-based robust control of robot manipulators. *IEEE Transactions on Control Systems Technology*, 1996, **4**(4): 384∼393

22 Slotine J J E, Li W. *Applied Nonlinear Control*. New Jersey: Prentice Hall, 1991

23 Khalil H. *Nonlinear Systems*. New Jersey: Prentice Hall, 2002

LIU Shi-Cai Ph. D. candidate at Shenyang Institute of Automation, Chinese Academy of Sciences. He received his bachelor degree from Wuhan University of Technology in 2001. His research interest covers mobile robot modeling and control. Corresponding author of this paper. E-mail: liushicai@sia.ac.cn

TAN Da-Long Professor at Shenyang Institute of Automation, Chinese Academy of Sciences. He received his bachelor degree from Tsinghua University in 1963. His research interest covers autonomous robots and applications of AI, and robotics to the industry and space probe.
E-mail: dltan@sia.cn

LIU Guang-Jun Tenured associate professor at Department of Aerospace Engineering, Ryerson University, Canada. He received his bachelor degree from University of Science and Technology of China in 1984, master degree from Shenyang Institute of Automation, Chinese Academy of Sciences in 1987, and Ph. D. degree from University of Toronto in 1996, respectively. His research interest covers control systems, robotics, mechatronics, and aircraft systems. E-mail: gjliu@ryerson.ca